separations

MDPI

Article

Fluorinated Poly(ionic liquid)s Coated Superhydrophobic Functional Materials with Efficient Oil/Water Separation Performance

Fumin Shen [1,†], Xuna Cheng [2,†], Shunyang Yao [2,*] and Yuanchao Pei [3,*]

[1] School of Pharmacy, Xinxiang University, Xinxiang 453003, China; ayssfm@163.com
[2] College of Forestey, Henan Agricultural University, Zhengzhou 450002, China; bfchengxuna@163.com
[3] School of Chemistry and Chemical Engineering, Henan Normal University, Xinxiang 453007, China
* Correspondence: yaosy0209@163.com (S.Y.); ycpei@htu.edu.cn (Y.P.)
† These authors contributed equally to this work.

Abstract: There is an urgent need to develop new and improved oil-water separation materials with high stability and reusability for the cleanup of oily environmental pollutants. Here, fluorinated poly(ionic liquid)s were synthesized and their structure and property were characterized by nuclear magnetic resonance spectroscopy, Fourier transform infrared spectroscopy and thermogravimetric analysis. These fluorinated poly(ionic liquid)s were proposed as superhydrophobic coating on different metallic substrates through the combination of tethering fluorine groups in the PIL's cation and anion exchange, and the superhydrophobic coating showed compactly stacked morphology under scanning electron microscope. The results of surface wettability experiments indicated that nearly all the fabricated materials showed a water contact angle larger than 150°, which is devoted to superhydrophobic nature. Moreover, for longer alkyl chain ILs and materials with smaller pore sizes, the water contact angle can be increased. At the same time, the fabricated superhydrophobic material exhibits a relatively high oil phase permeate flux, benefiting from the loose fibrous structure. Take the PIL@SSM300 for instance, the permeate fluxes were reached as high as 374,370 $L \cdot m^{-2} \cdot h^{-1}$, 337,200 $L \cdot m^{-2} \cdot h^{-1}$ and 302,013 $L \cdot m^{-2} \cdot h^{-1}$ for petroleum ether, hexane and cyclohexane, respectively. Instead, water is effectively repelled from the superhydrophobic surface. These virtues make the fabricated superhydrophobic material an effective membrane for oil/water separation under gravity. The separation efficiency and water contact angle are nearly unaffected after at least 20 cycles, confirming the excellent robustness of the coatings. These efficient poly(ionic liquid)s-based superhydrophobic materials possessed the potential to be used for oil/water separation.

Keywords: poly(ionic liquid)s; functional material; oil/water separation; water contact angle; superhydrophobicity

check for updates

Citation: Shen, F.; Cheng, X.; Yao, S.; Pei, Y. Fluorinated Poly(ionic liquid)s Coated Superhydrophobic Functional Materials with Efficient Oil/Water Separation Performance. *Separations* **2023**, *10*, 405. https://doi.org/10.3390/separations10070405

Academic Editors: Catarina Seiça Neves, Filipa A. Vicente, Jorge F. B. Pereira and João Henrique Picado Madalena Santos

Received: 17 May 2023
Revised: 5 July 2023
Accepted: 12 July 2023
Published: 14 July 2023

1. Introduction

Oily water is one of the major environmental issues so far, caused by different industries and production processes, such as oil spills, household sewage, pharmaceutical production and industrial oily wastewater [1–5]. Oily water usually contains toxic chemicals, which can pose serious risks to ecosystems and people's health. Therefore, the development of effective methods to remove oil from water before it is discharged into the environment has become an emerging and urgently necessary critical issue. Different techniques and related materials have been reported to remove oil from water, including gravity separation, skimming flotation, filtration, adsorption, de-emulsification and others [6–13]. These techniques and related materials have their own advantages and disadvantages. Developing efficient methodology or cost-effective, environmentally friendly and recyclable materials is highly desirable. Currently, filtration and adsorption have attracted

attention as efficient oil/water separation methods thanks to their convenience, low cost and environmental friendliness [14,15].

Materials with different superwetting properties towards oil and water (e.g., superhydrophobic or superhydrophilic surface) have recently attracted increasing attention in oil/water separation. Metallic mesh, cotton fabrics and textile membranes stand for the most studied superwetting materials by the surface modification. Furthermore, novel porous material-based superwetting materials, such as metal organic frameworks (MOFs), graphene, carbon nanotube, hydrogel and covalent organic frameworks (COFs), have also been proposed as an efficient separation strategy [16–20]. These smart material-based membrane techniques have received high research interest for the efficient separation processes with the characteristics of low energy consumption and simple separation devices. The membrane acts as a barrier, allowing the selective transport of oil or water from one side to the other. The main driving force for the passage of water or oil through the membrane mainly depends on the pressure or surface porosity. In the presence of gravity, surface porosity is particularly important. Smart hybrid membrane materials with large pore sizes and high flow rates are preferred for the separation of oily water [21]. The surface engineering and morphology of solid surfaces have a direct influence upon the wetting behavior [22,23]. Meanwhile, shaping with various technologies and coating on a substrate is demonstrated as an effective strategy to improve recycling and handling. Superhydrophobic materials have aroused broad interest because of their facile fabrication and effective separation oil/water mixtures or emulsions by selective filtration or absorption [5]. The design and construction of superhydrophobic coatings with controllable material surface wettability has been demonstrated as an effective method for enhancing the separation performance. However, the modification of the superhydrophobic surface of functional materials and the improvement of durability remain challenging in practical applications.

To address these issues, many efforts have been aimed at fabricating robust and versatile superhydrophobic materials suitable for practical environments. Mohamed and co-workers reported a biological MOF constructed of copper and aspartic acid to improve the surface roughness of the pristine textile fabric [24]. A water contact angle of 158° was observed for the obtained superhydrophobic textile fabric. The results imply that the superhydrophobic textile fabric exhibits excellent oil-water mixture and emulsion separation performance, oil absorption capacity, chemical stability, mechanical abrasion resistance and high flux rates. Meng and co-workers developed superhydrophobic wrinkled ZIF-8@rGO microspheres by intercalating the crumpled reduced graphene oxide (rGO) nanosheets in the well-dispersed ZIF-8 nanoparticles [25]. The wrinkled ZIF-8@rGO microspheres exhibit fast absorption rates and high sorption selectivity of oily compounds from water thanks to their super wettability and rich meso/microporosity. Cui et al. report controllable hydrophobicity and processability two-dimensional robust fluorinated COFs by condensation of triamines with fluorine and/or isopropyl groups and perfluorodialdehyde [26]. A superhydrophobic stainless-steel mesh (SSM) substrate coated by fluorinated COFs shows water contact angles of 111.5–145.8° and excellent water-resistance and self-cleaning properties. Bhaumik et al. developed a superhydrophobic COF through Schiff-base condensation reaction and 1,4-conjugate addition reactions [27]. The tailorable wettability of the prepared COF significantly enhances the oil absorption capacity under diverse and harsh conditions.

On solid surfaces, fluorinated coatings are an effective strategy to convert hydrophilic surfaces into hydrophobic ones, and they can easily find a wide range of applications, from electronic devices to membranes and nanocomposite materials. Despite being an indispensable role in some scientific fields, it is necessary to pay attention to the toxicity of long-chain linear perfluoroalkyl compounds ($n > 8$) to environment [28–31]. Ionic liquids (ILs), featuring non-volatility and non-flammability, excellent thermal and chemical stability, tunable structure and property, and high solvency power, etc., had aroused wide public concern in the scientific and industrial fields [32–37]. The tunable nature of ILs offers a promising way to fabricate fascinating functional materials to meet the needs of specific applications. Poly(ionic liquids) (PILs), as fascinating materials, have the desirable tunability of

physico-chemical property through the selection of the right anions or tethering functional groups in the main framework [38–40]. Smart separation materials coated by functional PIL are considered a vital alternative for oil-water separation [41–45]. So far, PIL-coated functional membrane materials with switchable hydrophilic/hydrophobic surfaces have been successfully fabricated by anion exchange or functional group modification on the PIL backbone. For example, Song and co-workers designed several porous hypercrosslinked poly(ionic liquid)s with high stability and reusability for oil-water separation [41]. The hydrophobicity of PIL materials can be tuned by the choice of different auxiliary crosslinkers. Zhao et al. reported a series of poly(ionic liquid) coated cotton fabric, cotton ball and nylon fabric intelligent materials [42]. A switchable superhydrophilic/superhydrophobic capability and an efficient oil-water separation performance have been observed for these materials. However, superhydrophobicity was difficult to achieve through simple ion exchange, where surfaces tend to switch after repeated and long-term use. There is an urgent need to develop superhydrophobic functional materials with high stability and durability for the cleanup of oily environmental pollutants. Recently, functionalization of ILs with the addition of a fluoro-alkyl chain to the cation structure is of particular interest due to their broad range of potential applications [30].

In this case, the combination of tethering fluorine groups in the PIL cation and anion exchange enables a flexible approach to fabricate robust superhydrophobic surfaces. Two ILs with different alkyl chain lengths were synthesized and subsequently coated on the surface of stainless-steel mesh and nickel foam metallic substrates by in situ polymerization and ion exchange. The wettability of the fabricated superhydrophobic material was examined by means of the water contact angle and permeation experiments. In addition, the variation of the permeate fluxes of the materials with the structure of the ILs and crosslinkers was investigated. These superhydrophobic materials have been demonstrated to be an effective oil-water separation material with the merits of excellent reusability, cost-effectiveness and high stability in the oil-water separation process.

2. Materials and Methods

2.1. Materials

1H,1H,2H,2H-tridecafluoro-n-octyl iodide (97.0%) and 1H,1H,2H,2H-perfluorodecyl iodide (98.0%) were obtained from TCI (Japan). 1-Vinylimidazole (98%), $LiTf_2N$ (99%) and 2,2′-azoisobutyronitrile (99%) were obtained from JK Chemicals. Petroleum ether (AR), cyclohexane (99.9%), hexane (99%), divinylbenzene (DVB) and other organic solvents were acquired from Adamas. All reagents were used directly without any further purification.

2.2. Synthesis of the Ionic Liquids Monomers

Fluorinated IL monomers are synthesized by a two-stage process of alkylation and anion exchange. Take the case of $[C_8H_4F_{13}mim]I$, 1-vinylimidazole and 1H,1H,2H,2H-tridecafluoro-n-octyl iodide were mixed with a small amount of toluene and transferred into a flask with the molar ratio of 1:1.1 under Ar atmosphere at 80 °C for one week. Then, the crude ILs were washed with toluene and diethyl ether, and solvent was removed by rotatory evaporator under vacuum at 60 °C. The product $[C_8H_4F_{13}mim]I$ was obtained. $[C_{10}H_4F_{17}mim]I$ was synthesized through the same procedure as $[C_8H_4F_{13}mim]I$. The structure of all the fluorinated ILs was confirmed by the nuclear magnetic resonance spectroscopy (^{1}H NMR and ^{19}F NMR, AV-600 Bruker) and spectra given in the supporting information (Figures S1 and S2) and as follows.

$[C_8H_4F_{13}vim]I$: ^{1}H NMR (600 MHz, DMSO-d_6, ppm): 9.57 (s, 1H, -N-CH=N-),8.21 (s, 1H, -N-CH), 8.02 (s, 1H, -N-CH), 7.31–7.35 (dd, 1H, -N-CH), 5.94–5.97 (dd, 1H, -N-CH), 5.45–5.46 (dd, 1H, -N-CH), 4.58–4.61 (t, 2H, -CH_2-), 3.01–3.10 (m, 2H, -CH_2-); ^{19}F NMR (600 MHz, DMSO-d_6, ppm): 80.25–80.29 (t, 3F, -CF_3-), 113.08–113.21 (m, 2F, -CF_2-), 121.70 (s, 2F, -CF_2-), 122.66 (s, 2F, -CF_2-), 123.20–123.23 (s, 2F, -CF_2-), 125.76–125.82 (s, 2F, -CF_2-).

$[C_{10}H_4F_{17}vim]I$: ^{1}H NMR (600 MHz, DMSO-d_6, ppm): 9.60 (s, 1H, -N-CH=N-), 8.23 (t, 1H, -N-CH), 8.03–8.04 (s, 1H, -N-CH), 7.33–7.37 (dd, 1H, -N-CH), 5.95–5.98 (dd, 1H, -N-CH),

5.47–5.48 (dd, 1H, -N-CH), 4.60–4.63 (t, 2H, -CH_2-), 3.04–3.08 (m, 2H, -CH_2-), ^{19}F NMR (600 MHz, DMSO-d_6, ppm): 80.17–80.21 (t, 3F, -CF_3-), 113.07–113.13 (m, 2F, -CF_2-), 121.43 (s, 2F, -CF_2-), 121.67 (s, 4F, -CF_2-CF_2-), 122.44 (s, 2F, -CF_2-), 123.16 (s, 2F, -CF_2-), 125.68–125.73 (s, 2F, -CF_2-).

2.3. Synthesis of the Superhydrophobic Materials Coated with Fluorinated Poly(ionic liquid)s

Commercial stainless-steel mesh (SSM, 300 and 500 mesh) and nickel foam (NF, 0.3 mm and 1.0 mm) were cut into pieces and washed with ethanol and acetone prior to use. Subsequently, the small pieces of SSM and NF were immersed in aqueous solution of 1.0 M HCl for ultrasonic washing. Take the PIL-1@SSM300-D for instance, 1.0 g [$C_8H_4F_{13}$vim]I monomer was dissolved into 5 mL ethanol containing 0.1 g AIBN, an appropriate amount of DVB and a piece of cleaned SSM. After several cycles of vacuum degassing in liquid nitrogen, the reaction was performed in the Schlenk line at 70 °C for about one day in N_2 atmosphere. Subsequently, the composite was washed with ethanol and dried at reduced pressure at 60 °C. The above material was immersed into 10 mL $LiTf_2N$ aqueous solution (0.1 mol·L^{-1}) with stirring for about 12 h to exchange their anions. The material is then immersed in fresh water to remove impurities. After that, the obtained PIL-1@SSM300-D material was dried at 70 °C for 24 h. PIL-1@SSM500-D, PIL-1@NF0.3-D, PIL-1@NF1.0-D, PIL-2@SSM300-D, PIL-2@SSM500-D, PIL-2@NF0.3-D and PIL-2@NF1.0-D were fabricated using the same protocol. For comparison, superhydrophobic materials without adding crosslinking agent were also synthesized, which were named PIL-1@SSM300, PIL-1@SSM500, PIL-1@NF0.3, PIL-1@NF1.0, PIL-2@SSM300, PIL-2@SSM500, PIL-2@NF0.3 and PIL-2@NF1.0, respectively.

2.4. Characterization of the Superhydrophobic Materials

Nuclear magnetic resonance (AVANCE-600, Bruker, Billerica, MA, USA) and Fourier transform infrared spectroscopy (FTIR) 400F spectrophotometer (PerkinElmer, Waltham, MA, USA) were suggested to verify the structure of synthesized IL monomers. Thermal decomposition temperature (T_d) of the PIL coating material was determined by STA 449C thermal analyzer (NETZSCH, Selb, Germany). The morphology of the materials was revealed through field emission scanning electron microscope (SEM) with the operating voltage of 10.0 KV (SU8010). The static water contact angle was examined by the contact angle instrument (DSA25S, KRUSS, Hamburg, Germany). The X-ray diffraction (XRD) pattern of samples was conducted on X'Pert3 Powder X-ray powder diffractometer. The Cu target Kα ray was used as the diffraction source with a scanning range of 10°–80°. X-ray photoelectron spectra (XPS, ESCALAB250Xi) were used to examine the chemical compositions of the material surface by using a monochromatic Al-Kα X-ray source for in-depth understanding of elemental composition and chemical state.

2.5. Separation Performance of the Superhydrophobic Materials

PILs coated superhydrophobic material was sandwiched between two glass tubes in vertical position and sealed with a silicone ring (Figure 1a). Three model oils, petroleum ether, cyclohexane and hexane, were used in this study. The 20–100 mL of oil is slowly placed into the upper tube (height: 15 cm) and then the oil phase is rapidly penetrated by gravity. The permeate fluxes (F, L·m^{-2}·h^{-1}) of the oil phase were determined by the following equation:

$$F = \frac{V}{St} \tag{1}$$

where S (m^2) and t (h) are the effective permeate area and separate time, respectively. All the permeate flux measurements data were expressed as the mean ± standard deviation of at least three independent tests.

For the oil-water separation, a home-made u-type separation device was used (Figure 1b). The oil-water mixtures (volume ratio 1:1) were added into the left part, the water (colored with methylene blue) was rejected by the superhydrophobic material and oil was penetrated

into the right part. The separation efficiency (R) of the oil phase was calculated via the following equation:

$$R = \frac{m_t}{m_0} \times 100\% \quad (2)$$

where m_t and m_0 are the final and initial mass of oil, respectively.

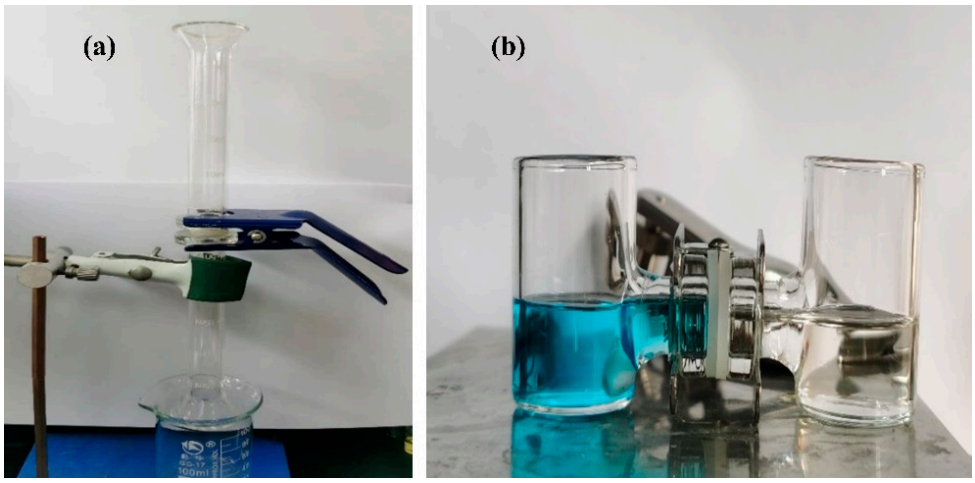

Figure 1. The device photos of permeate flux (**a**) and separation efficiency (**b**).

3. Results and Discussion

3.1. Fabrication and Characterization of the PIL Coated Materials

The structure of the monomers of ILs was confirmed by ^{1}H NMR and ^{19}F NMR. The detailed fabrication process of the material coated with PIL is shown in Figure 2a. A schematic of the synthesis of PILs is depicted in Scheme S1. PIL coatings are fabricated by thermal-initiated polymerization and subsequent anion exchange processes. The cleaned substrate is first immersed in a monomer solution. After subsequent polymerization, the PILs produce a circle of superhydrophobic coating around the fiber of the substrate. I^- anion of the PIL can be easily replaced by $[Tf_2N]^-$ by immersing the pristine PIL coated materials into $LiTf_2N$ aqueous solution for about 12 h at room temperature. The color of the final superhydrophobic material changes significantly from gray to light yellow. FTIR spectra of ionic liquid monomer $[C_8H_4F_{13}vim]I$, PIL-1 and PIL-2 are present in Figures 2b and S3. For $[C_8H_4F_{13}vim]I$, the characteristic absorption peaks of 3072 cm^{-1} and 1572 cm^{-1} belong to the stretching vibration of the C−H and C−C in imidazolium ring, respectively. The stretching vibration of the C=C bond is primarily situated at 1654 cm^{-1}. Two peaks are observed at 1041 cm^{-1} and 619 cm^{-1} which are attributed to the stretching vibration and bending vibration of the C−F bond, respectively. The FTIR results of PIL-1 indicate that the characteristic absorption peaks of monomer $[C_8H_4F_{13}vim]I$ remain in the PIL-1. However, no characteristic peak of C=C at 1654 cm^{-1} was found in the spectra of PIL-1, which verifies the successful synthesis of PIL from the ILs monomers.

Thermogravimetric analysis (TGA) of PIL and monomer are shown in Figures S4 and S5. Similar weight loss is observed for both ILs monomer and PILs. The higher decomposition temperature of the PIL exhibits superior thermal stability. PIL-2, with a longer alkyl chain length, exhibits higher thermal stability than that of PIL-1. The XRD pattern of PIL-1 with and without DVB is depicted in Figure 2c. A broad peak with expressive width at 2θ of 10–20° and 35–45° in the XRD pattern was observed for the PIL-1 without addition of DVB, which was predominantly originated from amorphous structure. After the addition of DVB, the PIL exhibits some sharp peaks, indicating that the PIL is well crystallized. XPS was used to characterize the surface chemical composition of PIL-1 before and after anion exchange. Figure 2d shows the XPS full spectrum of the PIL-1, showing that C1s, N1s, F1s and I3d peaks are all observed for PIL-1 before the anion exchange. It is noted that the characteristic peak of S2p appears after the anion exchange. The S

elements are derived from Tf_2N, indicating successful anion exchange by Tf_2N anions. In addition, the distinctive peak of I3d is significantly weaker. In order to illustrate the effect of anion exchange, the deconvolution of I3d before and after anion exchange is shown in Figure 2e. The I content in PIL-1 was 2.46 atomic% before the anion exchange and decreased to 0.27 atomic% after the anion exchange. This phenomenon can be explained by the successful anion exchange of the PIL coating.

SEM was suggested to determine the morphology of bare SSM and NF, PIL@SSM and PIL@NF. As shown in Figure 3a, the bare SSM exhibits a neat fibrous morphology and a smooth surface. In the SEM images of the PIL@SSM, a large number of PIL particles are compactly stacked with each other on the SSM surface, and the surface becomes rough. For the PIL@SSM-D, no significant change in the morphology of PIL@SSM-D was observed after the introduction of DVB. In addition, the diameter of the SSM fiber and the average pore size of SSM-300 were 40 μm and 44 μm, respectively. After the polymerization of ILs monomer, the diameter of SSM fiber rose to about 50 μm. Figure 3d shows a bare NF network with a smooth surface. Because the NF was built up layer by layer, the average pore size was about 200 μm. After the polymerization of the PIL on the NF fiber, a thicker polymeric coating is observed, as shown in the SEM images of Figure 3e,f. The surface roughness of the NF fiber increases. In summary, SEM images were used to characterize the morphology of the PIL coated material and also to show the enhanced roughness. The above results indicate the successful fabrication of the superhydrophobic materials coated with PIL. The superhydrophobic PIL coating effectively prevents water from passing through the mesh. The oil phase, meanwhile, passes rapidly through the lipophilic PIL coated mesh.

The key factor for the efficient separation of oil-water mixtures is the wettability of the material. The surface wettability is characterized by static water contact angle measurements. The static water contact angles for PIL@SSM and PIL@NF are depicted in Figures 4 and 5, respectively. For a bare SSM or NF, the surface is hydrophilic, and the water droplets are immediately spread out on the cleaned SSM or NF surface, and the angle of water considered to be 0°. Figure 4 showed that the static water contact angle of PIL-1@SSM300 is about 148.9° ± 0.8°, and it behaves as a superhydrophobic surface. In addition, the static water contact angle increases as the length of the alkyl chain of IL cation increases, which is related to the increased hydrophobicity of the longer alkyl chain. For example, the static water contact angle of PIL-1@SSM300 and PIL-2@SSM300 is about 148.9° ± 0.8° and 155.9° ± 1.1°, respectively. Meanwhile, the contact angles of oil on the surface of PIL@SSM are considered as 0° because the oil droplets are absorbed immediately by the materials. Moreover, hydrophobicity depends on the surface roughness or the pore size of the mesh. The pore size of SSM is 44 μm and 26 μm for 300 mesh and 500 mesh, respectively. Smaller pore sizes with smoother surfaces have higher water contact angles. Take the case of PIL-1@SSM, the static water contact angle of PIL-1@SSM300 and PIL-1@SSM500 is about 148.9° ± 0.8° and 151.2° ± 0.9°, respectively. Meanwhile, superhydrophobicity can be obtained by coating the SSM surface with PILs to increase the surface roughness. Water could spread into the surface of cleaned SSM, which means the water contact angle close to 0°. After coating of PILs, the water contact angle increased to about 150°. In addition, as shown in Figure 4, when DVB is used as crosslinking agent, the water contact angle of PIL-1@SSM300 increased from 148.9° ± 1.1° to 156.9° ± 1.1°, while the water contact angle of PIL-1@SSM500 increased from 151.2° ± 0.9° to 160.2° ± 1.0°. Superhydrophobicity is enhanced by the addition of a crosslinking agent. Similar findings have been observed in the PIL@NF material shown in Figure 5. For example, the water contact angle of PIL@NF increases with the length of the alkyl chain and with the addition of the crosslinking agent. The superhydrophobicity is mainly owing to the influence of functional groups on the crosslinking agent [41]. Due to the hydrophobic nature of DVB, the water contact angle is significantly increased after the addition of DVB. The results discussed above indicate the successful introduction of hydrophobic fluorinated PIL to the substrate.

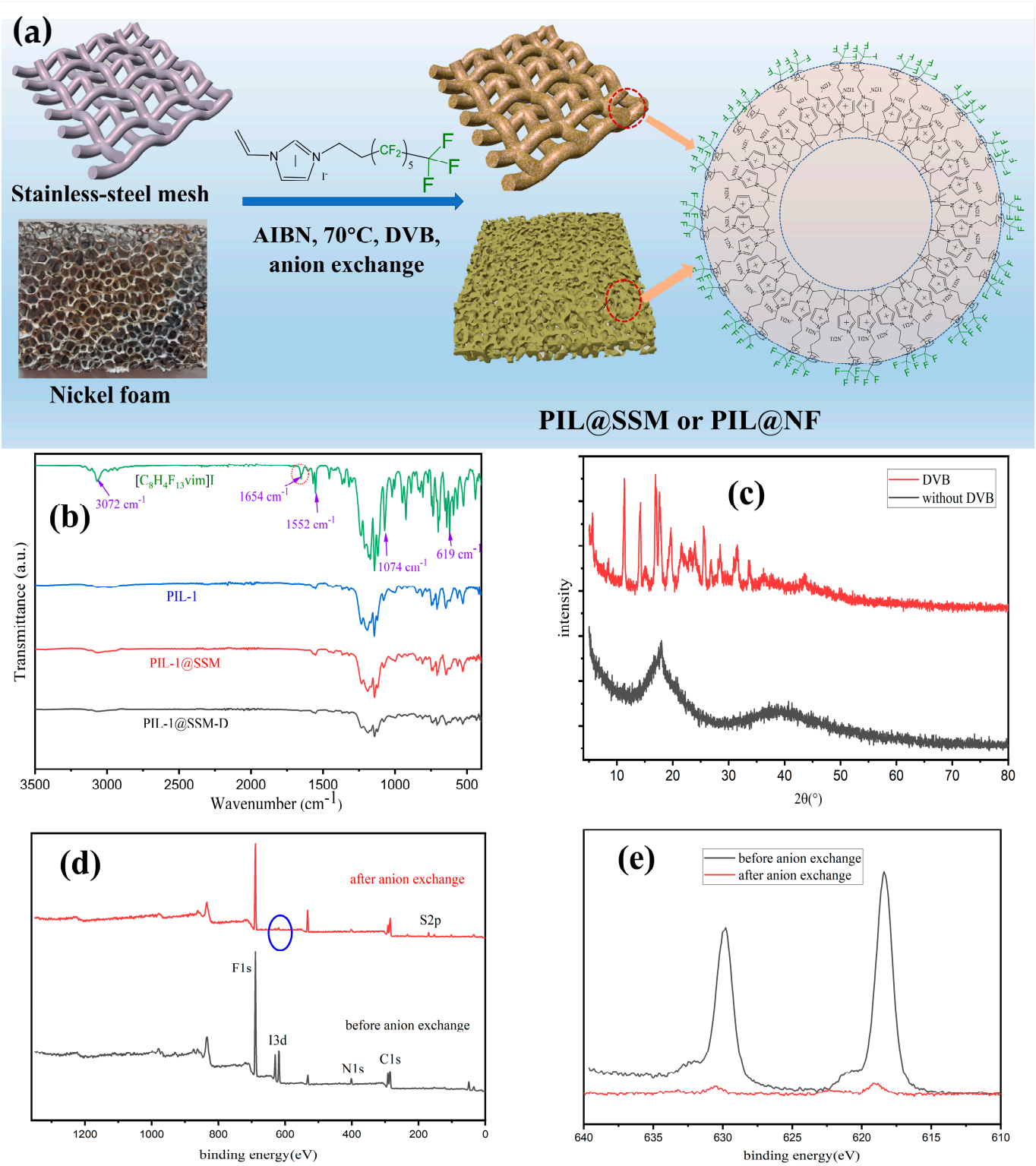

Figure 2. Schematic illustration for the preparation process (**a**), FTIR spectra of $[C_8H_4F_{13}vim]I$ monomer and PIL−1 composites (**b**), XRD patterns of PIL−1 with and without DVB (**c**), XPS survey of PIL−1 before and after anion exchange (**d**) and the I3d XPS spectrum of the PIL−1 before and after anion exchange (**e**). The blue circle in subfigure (**d**) show the position of I3d.

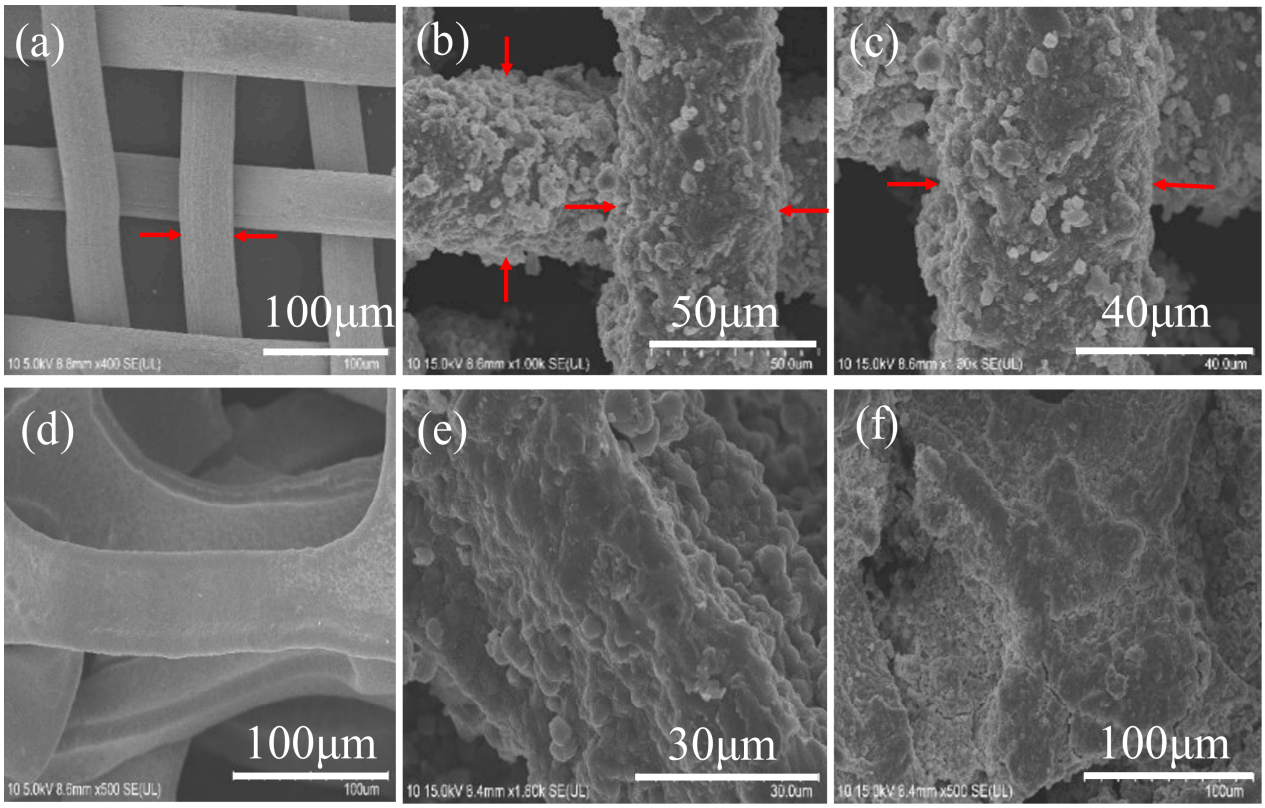

Figure 3. SEM pictures of PIL coated materials. (**a**) SSM-300, (**b**) PIL-1@SSM-300, (**c**) PIL-1@SSM-300-D, (**d**) 0.3 mm NF, (**e**) PIL-1@ NF0.3 and (**f**) PIL-1@ NF0.3-D. The distance between two red arrows represents the diameter of the SSM fiber.

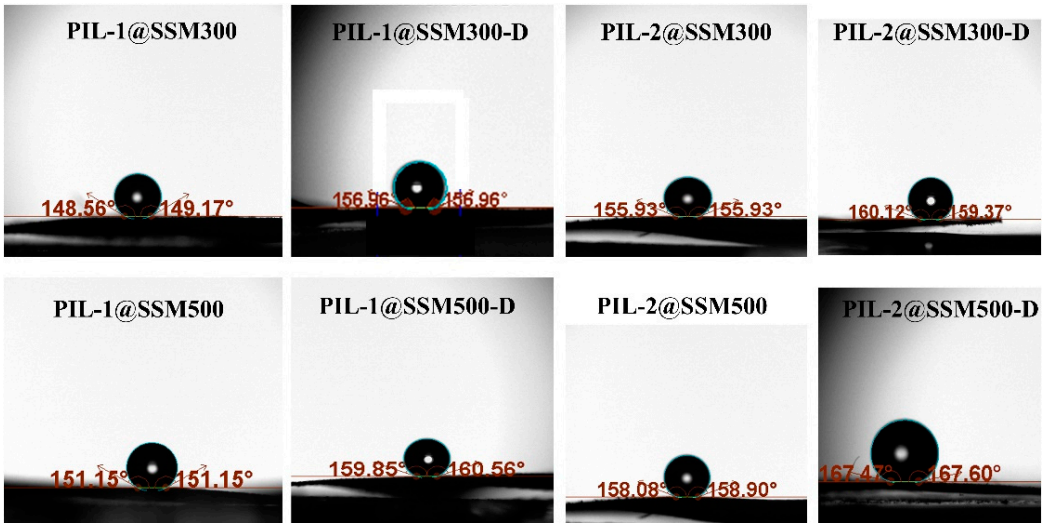

Figure 4. Static water contact angle of PIL@SSM.

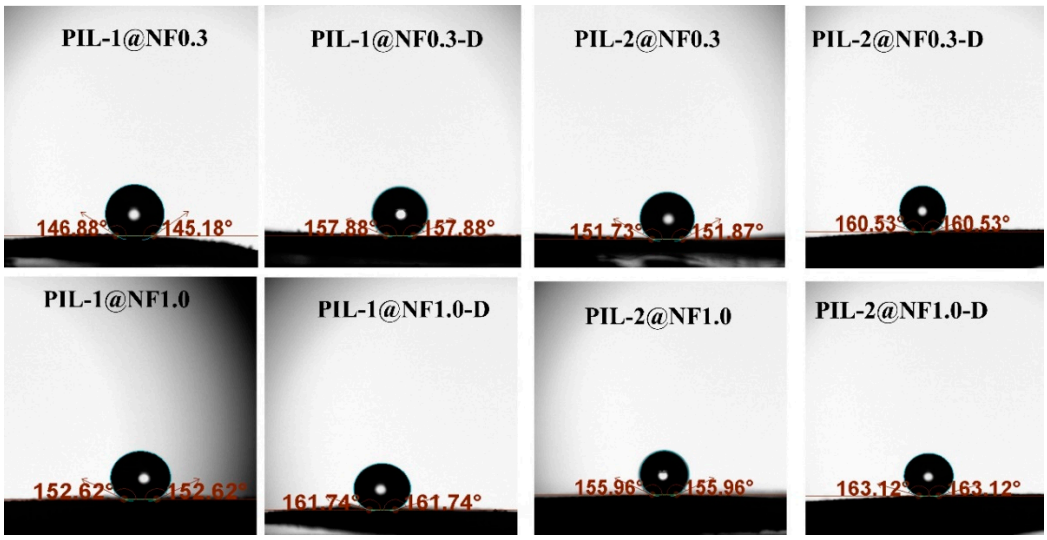

Figure 5. Static water contact angle of PIL@NF.

3.2. The Permeate Flux of the Oil Phase

Superhydrophobic materials, also known as oil removing materials, may allow the oil phase to permeate the material while water is repelled. The wettability of the surface by oil phase is examined by the permeate flux (F, $L \cdot m^{-2} \cdot h^{-1}$). A gravity-driven filtration system is suggested to examine the permeate flux. In general, the permeate flux of a solvent depends on a number of factors such as density, viscosity, polarity and wettability. The higher permeate flux of the oil phase requires a higher density, lower polarity, lower viscosity and superior wettability of the superhydrophobic material. Three model oils, petroleum ether, cyclohexane and hexane, are permeated by gravity through a superhydrophobic material. The oil fluxes passed through the superhydrophobic material are listed in Table 1. The results indicate that these superhydrophobic materials have excellent permeability to different solvents, even though the density of these oil phases is lower than that of water. As an example of PIL-1@SSM300, the fluxes of petroleum ether, hexane and cyclohexane were 374,370 $L \cdot m^{-2} \cdot h^{-1}$, 337,200 $L \cdot m^{-2} \cdot h^{-1}$, 302,013 $L \cdot m^{-2} \cdot h^{-1}$, respectively. The sequence of fluxes agrees with the polarities of oil phase, while the order of polarities of oil phase is petroleum ether < hexane < cyclohexane as shown in Figure 6a,b. The weak polarity of the oil phase favors rapid passing through the superhydrophobic material. The materials fabricated in this work have similar results. Moreover, the structure of the substrate also plays a key role in the penetration process. As an example of petroleum ether, its permeate fluxes decrease from 374,370 $L \cdot m^{-2} \cdot h^{-1}$ to 122,000 $L \cdot m^{-2} \cdot h^{-1}$, with the mesh of SSM increasing from 300 to 500, while the pore size fell to 26 μm from 44 μm. Smaller pore sizes should of course increase the resistance, which in turn would lead to a significant decline in the permeate fluxes.

On the other hand, the effect of the alkyl chain length of the ILs on the oil phase fluxes has also been examined. Take the PIL@SSM300 as an example, the flux value of petroleum ether increases from 374,370 $L \cdot m^{-2} \cdot h^{-1}$ to 573,000 $L \cdot m^{-2} \cdot h^{-1}$ with the alkyl chain length increasing from PIL-1 to PIL-2. The PIL with longer alkyl chain length is more hydrophobic, while the affinity between the PIL and the oil phase is enhanced, which leading to a higher flux. Similar results exist in other materials. In general, crosslinking agents are helpful in producing crosslinking polymer chain networks. Although the water contact angle of PIL@SSM increases after the addition of the crosslinking agent, the permeation flux of the PIL@SSM-D eventually decreases. The reason for this phenomenon is attributed to the increased resistance to permeation after the addition of crosslinking agent.

Moreover, thicker materials are usually used to increase the permeation distance and resistance, and thus lead to smaller permeation fluxes. This is demonstrated by the results shown in Table 1 and Figure S6. Take the PIL-1@NF as an example, the permeation fluxes

values are 43,326 L·m^{-2}·h^{-1} and 37,922 L·m^{-2}·h^{-1} for PIL-1@NF0.3 and PIL-1@NF1.0, respectively. Due to the high porosity, the PIL@NF material can provide sufficient room for the storage of the oil phase. These materials can be used for rapid absorption of the oil droplets dispersed in the water phase.

Table 1. The permeate fluxes (F, L·m^{-2}·h^{-1}) for different oil phases of PIL-based materials and comparison with the literature data.

PIL−Based Materials	Petroleum Ether	Hexane	Cyclohexane	Ref.
PIL−1@SSM300	374,370 ± 15,310	337,200 ± 12,416	302,013 ± 9957	
PIL−1@SSM300-D	75,800 ± 1253	64,500 ± 910	44,310 ± 428	
PIL−1@SSM500	122,000 ± 1623	109,060 ± 1297	70,608 ± 543	
PIL−1@SSM500-D	45,090 ± 440	28,345 ± 175	19,836 ± 170	
PIL−2@SSM300	573,000 ± 35,960	362,000 ± 14,310	352,770 ± 13,591	
PIL−2@SSM300-D	377,450 ± 15,563	291,170 ± 9254	262,060 ± 7494	
PIL−2@SSM500	175,370 ± 3354	105,790 ± 1220	98,900 ± 1066	
PIL−2@SSM500-D	62,865 ± 860	50,590 ± 558	43,660 ± 416	
PIL−1@NF0.3	43,326 ± 409	41,603 ± 377	18,756 ± 154	
PIL−1@NF0.3-D	36,400 ± 288	27,330 ± 163	11,887 ± 110	
PIL−1@NF1.0	37,922 ± 314	28,793 ± 180	16,046 ± 114	
PIL−1@NF1.0-D	21,325 ± 198	18,350 ± 146	5521 ± 67	
PIL@cotton fabric		69,610		[42]
PIL@nylon fabric		12,123		[42]
PILM−1 or PILM−5	122,000	15,071		[44]
GO−PIL@cotton fabric		59,000		[45]
MWCNT@MTMS	126,400			[46]
TiO_2@SSM		7281		[47]
PDMS@PMMA		35,712		[48]
SLS@CNT	13,800	10,500		[49]
UA−co−VTMS@			8645	[50]
Ti3C_2Tx/PU	328,040		360,340	[51]

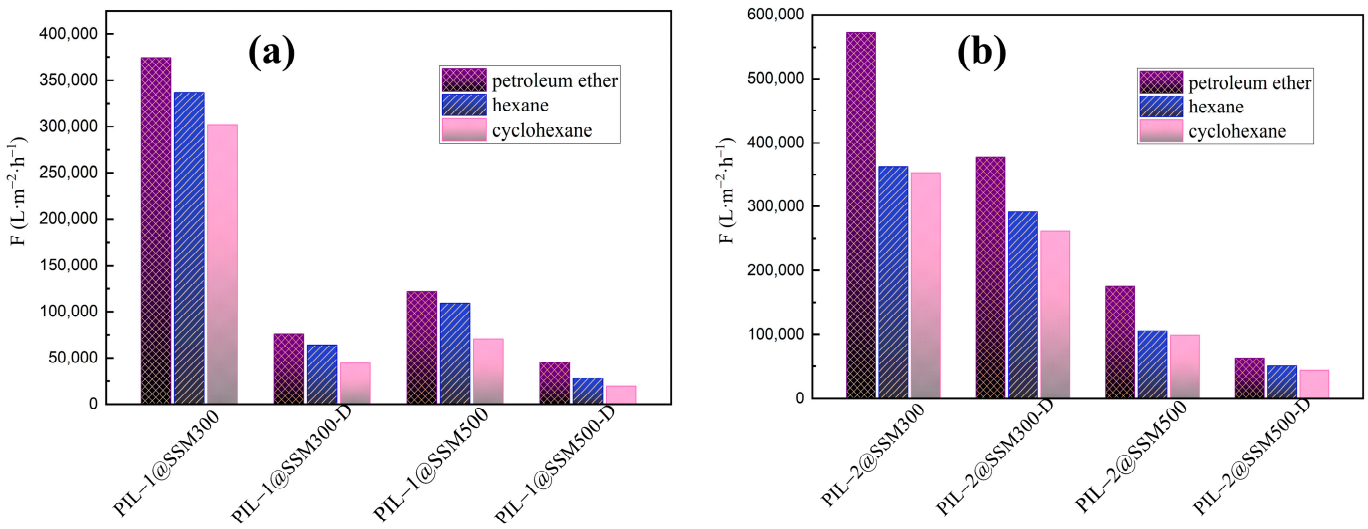

Figure 6. The permeate fluxes of oil phases for PIL−1@SSM (**a**) and PIL−2@SSM (**b**) composites.

3.3. Oil-Water Separation Performance

PIL-based superhydrophobic materials PIL@SSM and PIL@NF can be used to separate oil-water mixtures. An equal volume of oil and water is mixed and injected into the left part of the u-shaped device, where the superhydrophobic material is sandwiched between two glass tubes. The oil phase flows rapidly into the right part of the u-shaped device and the water phase is blocked. For comparison, both oil and water can pass quickly through the naked SSM or NF membrane. Continuous operation is easily realized by the immediate removal of the oil and water phases by the peristaltie pump. For ease of observation, the water phase is colored by methylene blue. The separation efficiency is intended to indicate the water removal performance of the fabricated superhydrophobic material. The separation efficiency can be calculated from the mass ratio of the oil phase

before and after permeation, and the results are shown in Figures 7 and S7 for PIL-1 and PIL-2 based materials, respectively. For all the oil-water mixtures, the separation efficiencies of petroleum ether, hexane and cyclohexane are all greater than 99%, indicating their promising separation performance for oil-water mixtures. The efficiency of the water is nearly 100%. At the same time, benefiting from the loose fibrous structure, it causes the acceleration of the separation process by gravity and is nearly free of the oil absorbed by the material. In addition, unlike the permeate flux, the separation efficiency is unaffected by the alkyl chain length, pore size and thickness of the NF.

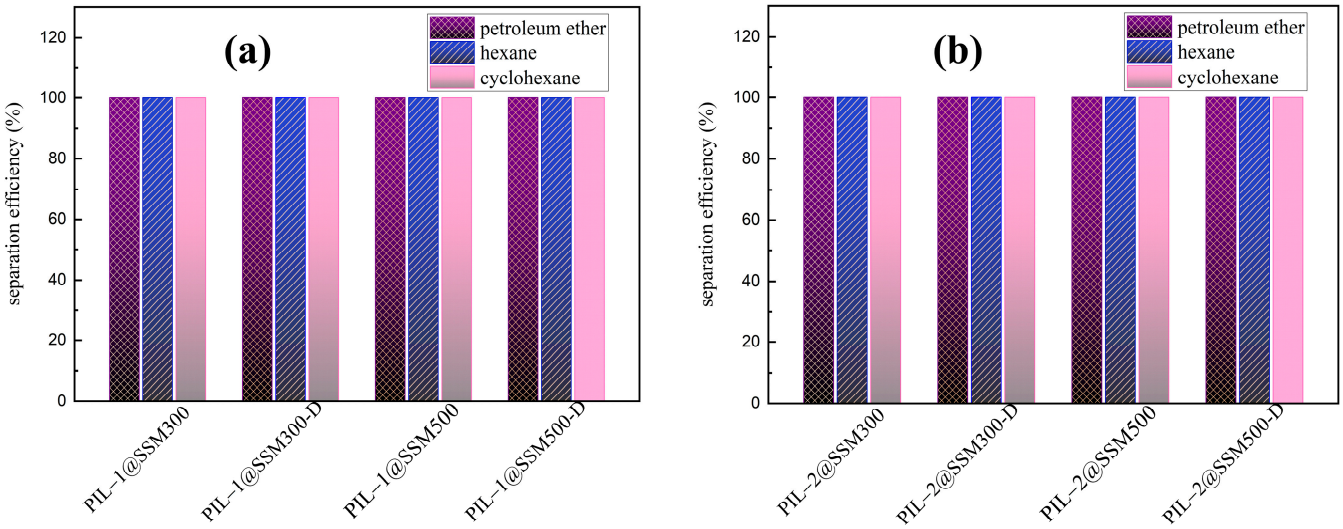

Figure 7. Separation efficiency of oil phase for PIL−1@SSM (**a**) and PIL−2@SSM (**b**) composites.

3.4. Recyclability of the Superhydrophobic Material

The durability of the superhydrophobic materials is of great importance when used in practical oil/water separation processes. As an example of a cyclohexane/water mixture, the separation efficiency of cyclohexane for PIL-1 based material is not affected after repeating for 20 times as shown in Figure S8. The water contact angle of these superhydrophobic materials after 20 cycles is shown in Figure 8. It is shown that the water contact angle does not decrease significantly for these materials compared to the pristine material. Take the PIL-1@SSM300 and PIL-1@NF0.3 for instance, the water contact angle was maintained 146.4° ± 0.9° and 146.0° ± 1.0°, respectively. Compared with the initial 148.9° ± 0.9° and 146.0° ± 1.0° for PIL-1@SSM300 and PIL-1@NF0.3, the water angle was not nearly affected, further confirming the superior robustness of the coatings. These materials still maintain large water contact angles due to their superhydrophobic nature. These results demonstrate the excellent reusability of PIL-based materials.

3.5. Separation Mechanism

Hydrophobic interactions and electrostatic attractions play vital roles in the sorption of crude oil from the oil-water mixtures [16]. For the model oils, such as petroleum ether, cyclohexane and hexane, the hydrophobic interactions are the main driving force. Superhydrophobic materials usually have a non-polar structure and long carbon chains. Fluorinated PILs coatings belong to the class of superhydrophobic materials, which are insoluble in water. Fluorinated PILs provide a distinct superhydrophobic surface on which densely packed carbon-fluorine (C−F) bonds [52] are present. The oil/water separation mechanism is tentatively proposed in Figure 9. Water molecules effectively repel from these densely C−F bonds on the superhydrophobic surface. On the contrary, superhydrophobicity, also known as lipophilicity, is a common affinity for oil molecules. This effect will cause rapid oil permeation across the superhydrophobic material.

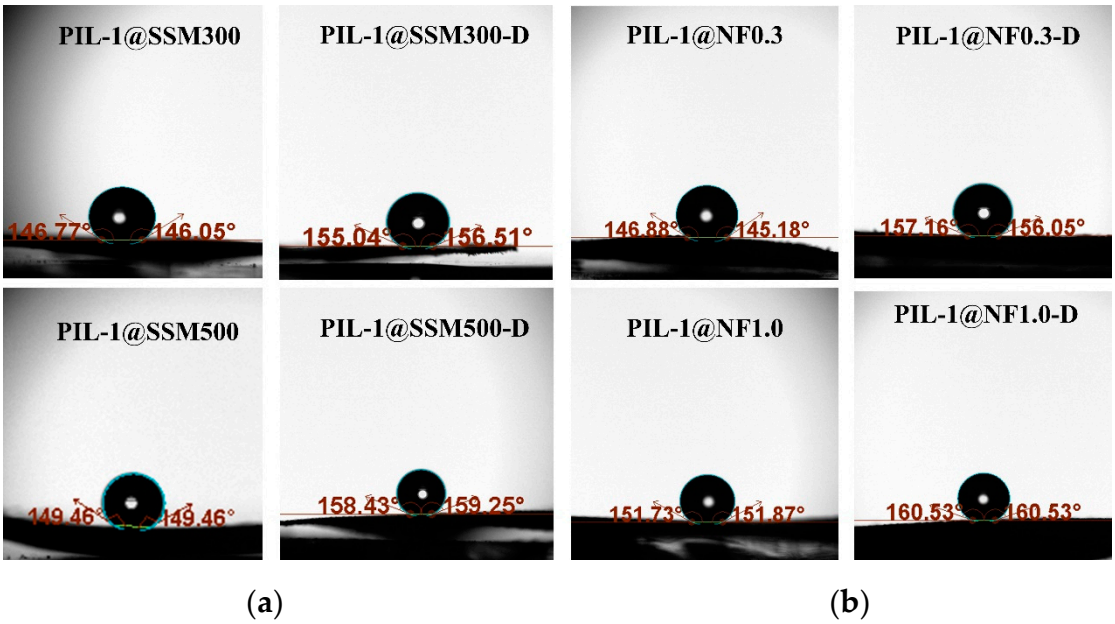

Figure 8. The water contact angle of PIL−1@SSM (**a**) and PIL−1@NF (**b**) compositesafter 20 times of oil/water separation recycle.

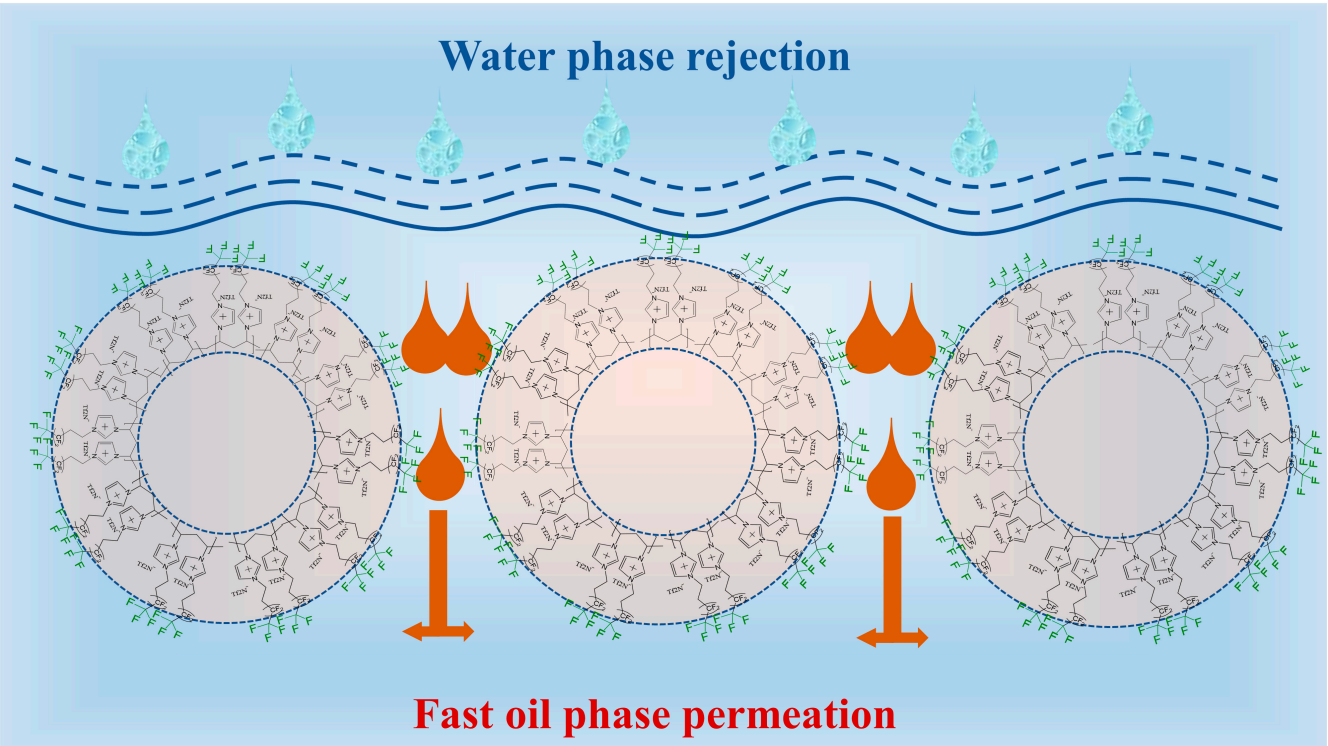

Figure 9. The proposed separation mechanism.

4. Conclusions

In this work, fluorinated poly(ionic liquid)s coated low-cost stainless-steel mesh and nickel foam superhydrophobic materials were prepared by in situ polymerization and ion exchange. The structure and thermal stability of poly(ionic liquid)s were characterized by NMR, FTIR and TGA methods. The SEM picture hints at the successful fabrication of compact stacked PIL coatings. In addition, nearly all the fabricated materials showed a water contact angle larger than 150°, which is devoted to superhydrophobic nature. Longer

alkyl chain ILs coated materials exhibit larger water contact angles. At the same time, the water contact angle can be increased for materials with smaller pore sizes and with the addition of a crosslinking agent. These fabricated superhydrophobic materials exhibit relatively high oil phase permeate fluxes, benefiting from the loose fibrous structure. Instead, water is effectively repelled from the superhydrophobic surface. Systematic oil/water separation experiments have shown that the fabricated superhydrophobic materials exhibit excellent oil/water separation efficiency under gravity, even for low density oil phases. The separation efficiency and water contact angle are nearly unaffected after at least 20 times recycle, indicating excellent reusability. These poly(ionic liquid)s-based superhydrophobic materials could be suggested as efficient absorbents for oil/water separation.

Supplementary Materials: The following supporting information can be downloaded at: https://www.mdpi.com/article/10.3390/separations10070405/s1, Scheme S1. The schematic of the reaction of PIL−1 with and without DVB. Figure S1: ^{1}H NMR and ^{19}F NMR spectra of [$C_8H_4F_{13}$vim]I; Figure S2: ^{1}H NMR and ^{19}F NMR spectra of [$C_{10}H_4F_{17}$vim]I; Figure S3: FTIR spectra of [$C_{10}H_4F_{17}$vim]I; Figure S4: TGA curves of [$C_8H_4F_{13}$vim]I and PIL−1; Figure S5: TGA curves of [$C_{10}H_4F_{17}$vim]I and PIL−1; Figure S6: The permeate flux of oil phase for different materials; Figure S7: Separation efficiency of oil phase for different materials; Figure S8: Separation efficiency of oil phase for different materials at least 20 times recycle.

Author Contributions: F.S.: conceptualization, investigation, writing—original draft preparation. X.C.: visualization, investigation, methodology, writing—original draft preparation. S.Y.: conceptualization, writing—review and editing, supervision. Y.P.: conceptualization, writing—review and editing, supervision, funding acquisition. All authors have read and agreed to the published version of the manuscript.

Funding: This study was supported by the Key Scientific Research Projects of Colleges and Universities in Henan Province (21A150026).

Data Availability Statement: All data have been presented in the paper and in Supplementary Materials.

Conflicts of Interest: The authors declare no conflict of interest.

References

1. Xiang, B.; Sun, Q.; Zhong, Q.; Mu, P.; Li, J. Current research situation and future prospect of superwetting smart oil/water separation materials. *J. Mater. Chem. A* **2022**, *10*, 20190–20217. [CrossRef]
2. Shi, G.; Shen, Y.; Mu, P.; Wang, Q.; Yang, Y.; Ma, S.; Li, J. Effective separation of surfactant-stabilized crude oil-in-water emulsions by using waste brick powder-coated membranes under corrosive conditions. *Green Chem.* **2020**, *22*, 1345–1352. [CrossRef]
3. Lee, C.H.; Tiwari, B.; Zhang, D.Y.; Yap, Y.K. Water purification: Oil–water separation by nanotechnology and environmental concerns. *Environ. Sci. Nano* **2017**, *4*, 514–525. [CrossRef]
4. Gupta, R.K.; Dunderdale, G.J.; England, M.W.; Hozumi, A. Oil/water separation techniques: A review of recent progresses and future directions. *J. Mater. Chem. A* **2017**, *5*, 16025–16058. [CrossRef]
5. Chu, Z.; Feng, Y.; Seeger, S. Oil/Water Separation with Selective Superantiwetting/Superwetting Surface Materials. *Angew. Chem. Int. Ed.* **2015**, *54*, 2328–2338. [CrossRef]
6. Wang, C.F.; Huang, H.C.; Chen, L.T. Protonated Melamine Sponge for Effective Oil/Water Separation. *Sci. Rep.* **2015**, *5*, 14294. [CrossRef]
7. Halim, A.; Ernawati, L.; Ismayati, M.; Martak, F.; Enomae, T. Bioinspired cellulose-based membranes in oily wastewater treatment. *Front. Environ. Sci. Eng.* **2022**, *16*, 94. [CrossRef]
8. Chen, B.; Zhang, R.; Fu, H.; Xu, J.; Jing, Y.; Xu, G.; Wang, B.; Hou, X. Efficient oil–water separation coating with robust superhydrophobicity and high transparency. *Sci. Rep.* **2022**, *12*, 2187. [CrossRef] [PubMed]
9. Kota, A.K.; Kwon, G.; Choi, W.; Mabry, J.M.; Tuteja, A. Hygro-responsive membranes for effective oil–water separation. *Nat. Commun.* **2012**, *3*, 1025. [CrossRef]
10. Huang, K.; Rowe, P.; Chi, C.; Sreepal, V.; Bohn, T.; Zhou, K.-G.; Su, Y.; Prestat, E.; Pillai, P.B.; Cherian, C.T.; et al. Cation-controlled wetting properties of vermiculite membranes and its promise for fouling resistant oil–water separation. *Nat. Commun.* **2020**, *11*, 1097. [CrossRef]
11. Fan, Q.; Lu, T.; Deng, Y.; Zhang, Y.; Ma, W.; Xiong, R.; Huang, C. Bio-based materials with special wettability for oil-water separation. *Sep. Purif. Technol.* **2022**, *297*, 121445. [CrossRef]
12. Li, Z.; Wang, M.; Li, Y.; Ren, J.; Pei, C. Effect of cellulose nanocrystals on bacterial cellulose hydrogel for oil-water separation. *Sep. Purif. Technol.* **2023**, *304*, 122349. [CrossRef]

13. Ma, Z.; Han, Y.; Xing, X.; Zhu, H.; Wang, Q.; Wang, X. Highly efficient oil–water separation of superhydrophobic cellulose II aerogel based on dissolution and regeneration of cotton in lithium bromide system. *J. Mol. Liq.* **2022**, *367*, 120543. [CrossRef]
14. Zhang, T.; Xiao, C.; Zhao, J.; Liu, X.; Huang, Y.; Ji, D. Graphite powder coated polyurethane sponge hollow tube as a high-efficiency and cost-effective oil-removal materials for continuous oil collection from water surface. *J. Appl. Polym. Sci.* **2020**, *137*, 48921. [CrossRef]
15. Srinivasan, A.; Viraraghavan, T. Oil removal from water using biomaterials. *Bioresour. Technol.* **2010**, *101*, 6594–6600. [CrossRef]
16. Shahmirzaee, M.; Abdi, J.; Hemmati-Sarapardeh, A.; Schaffie, M.; Ranjbar, M.; Khataee, A. Metal-organic frameworks as advanced sorbents for oil/water separation. *J. Mol. Liq.* **2022**, *363*, 119900. [CrossRef]
17. Lv, Y.; Xi, X.; Dai, L.; Tong, S.; Chen, Z. Hydrogel as a Superwetting Surface Design Material for Oil/Water Separation: A Review. *Adv. Mater. Interfaces* **2021**, *8*, 2002030. [CrossRef]
18. Chen, L.; Zhou, C.; Yang, H.; Lin, J.; Ge, Y.; Zhou, W.; Lu, C.; Tan, L.; Dong, L. Room-temperature fabrication of superhydrophobic covalent organic framework (COF) decorated cotton fabric for high-flux water-in-oil emulsion separation. *Chem. Commun.* **2021**, *57*, 11533–11536. [CrossRef] [PubMed]
19. Zaidi, S.A.; Mohamed, M.; Deyab, N. A simple method for developing efficient room temperature reduced graphene oxide-coated polyurethane sponge and cotton for oil-water separation. *Sep. Sci. Technol.* **2022**, *57*, 2596–2604. [CrossRef]
20. Huang, Z.; Luo, X.; Mi, Y.; Wu, G.; Wang, C.; Liu, L.; Ye, F.; Luo, Y. Magnetic recyclable carbon nanotubes and its demulsification performance in oily wastewater. *Sep. Sci. Technol.* **2021**, *56*, 150–2158. [CrossRef]
21. Ali, N.; Bilal, M.; Khan, A.; Ali, F.; Iqbal, H.M.N. Design, engineering and analytical perspectives of membrane materials with smart surfaces for efficient oil/water separation. *Trends Anal. Chem.* **2020**, *127*, 115902. [CrossRef]
22. Liu, M.; Wang, S.; Jiang, L. Nature-inspired superwettability systems. *Nat. Rev. Mater.* **2017**, *2*, 17036. [CrossRef]
23. Sam, E.K.; Liu, J.; Lv, X. Surface engineering materials of superhydrophobic sponges for oil/water separation: A review. *Ind. Eng. Chem. Res.* **2021**, *60*, 2353–2364. [CrossRef]
24. Mohamed, M.E.; Abd-El-Nabey, B.A. Fabrication of a biological metal–organic framework based superhydrophobic textile fabric for efficient oil/water separation. *Sci. Rep.* **2022**, *12*, 15483. [CrossRef]
25. Gu, J.; Fan, H.; Li, C.; Caro, J.; Meng, H. Robust Superhydrophobic/Superoleophilic Wrinkled Microspherical MOF@rGO Composites for Efficient Oil–Water Separation. *Angew. Chem. Int. Ed.* **2019**, *58*, 5297–5301. [CrossRef]
26. Liu, Y.; Li, W.; Yuan, C.; Jia, L.; Liu, Y.; Huang, A.; Cui, Y. Two-Dimensional Fluorinated Covalent Organic Frameworks with Tunable Hydrophobicity for Ultrafast Oil–Water Separation. *Angew. Chem. Int. Ed.* **2022**, *61*, e202113348. [CrossRef]
27. Ruidas, S.; Das, A.; Kumar, S.; Dalapati, S.; Manna, U.; Bhaumik, A. Non-Fluorinated and Robust Superhydrophobic Modification on Covalent Organic Framework for Crude-Oil-in-Water Emulsion Separation. *Angew. Chem. Int. Ed.* **2022**, *61*, e202210507. [CrossRef]
28. Dichiarante, V.; Milani, R.; Metrangolo, P. Natural surfactants towards a more sustainable fluorine chemistry. *Green Chem.* **2018**, *20*, 13–27. [CrossRef]
29. Verdia, P.; Gunaratne, H.Q.N.; Goh, T.Y.; Jacquemin, J.; Blesic, M. A class of efficient short-chain fluorinated catanionic surfactants. *Green Chem.* **2016**, *18*, 1234–1239. [CrossRef]
30. Diejomaoh Abafe, O.T.; Azim, M.M.; Martincigh, B.S.; Stark, A. Cation-fluorinated ionic liquids: Synthesis, physicochemical properties and comparison with non-fluorinated analogues. *J. Mol. Liq.* **2022**, *349*, 118104. [CrossRef]
31. Pei, Y.; Ma, J.; Song, F.; Zhao, Y.; Li, Z.; Wang, H.; Wang, J.; Du, R. Stable nanoreactors for material fabrication using the aggregation of fluorinated ionic liquid surfactants in ionic liquid solvents. *J. Mol. Liq.* **2022**, *366*, 120256. [CrossRef]
32. Pei, Y.; Zhang, Y.; Ma, J.; Fan, M.; Zhang, S.; Wang, J. Ionic liquids for advanced materials. *Mater. Today Nano* **2022**, *17*, 100159. [CrossRef]
33. Himani; Raman, A.P.S.; Singh, M.B.; Jain, P.; Chaudhary, P.; Bahadur, I.; Lal, K.; Kumar, V.; Singh, P. An update on synthesis, properties, applications and toxicity of the ILs. *J. Mol. Liq.* **2022**, *364*, 119989. [CrossRef]
34. Yuan, X.-Q.; Zhang, Y.-Q.; Li, Z.-Y.; Huo, F.; Dong, Y.-H.; He, H.-Y. Stimuli Responsive Ionic Liquids and the Regulation of Aggregation Structure and Phase Behavior. *Chin. J. Chem.* **2021**, *39*, 729–744. [CrossRef]
35. Zhang, Y.; Lu, F.; Yu, Y.; Su, L.; Gao, Y.; Zheng, L.; Gao, X. Amphiphile regulated ionic-liquid-based aqueous biphasic systems with tunable LCST and extraction behavior. *Colloids Surf. A Physicochem. Eng. Asp.* **2022**, *654*, 130172. [CrossRef]
36. Yuan, X.; Liu, J.; Wang, Y.; Jie, X.; Qin, J.; He, H. Ionic liquids enable highly efficient Knoevenagel reaction by dual-responsive emulsion microreactor. *Chem. Eng. J.* **2023**, *451*, 138941. [CrossRef]
37. Mahanty, B.; Mohapatra, P.K. Direct dissolution of metal oxides in ionic liquids as a smart strategy for separations: Current status and prospective. *Sep. Sci. Technol.* **2022**, *57*, 2792–2823. [CrossRef]
38. Zhang, S.; Zhuang, Q.; Zhang, M.; Wang, H.; Gao, Z.; Sun, J.; Yuan, J. Poly(ionic liquid) composites. *Chem. Soc. Rev.* **2020**, *49*, 1726–1755. [CrossRef] [PubMed]
39. Pei, Y.; Zhang, Y.; Ma, J.; Zhao, Y.; Li, Z.; Wang, H.; Wang, J.; Du, R. Carboxyl functional poly(ionic liquid)s confined in metal–organic frameworks with enhanced adsorption of metal ions from water. *Sep. Purif. Technol.* **2022**, *299*, 121790. [CrossRef]
40. Zhang, R.; Ahmed, A.; Yu, B.; Cong, H.; Shen, Y. Preparation, application and development of poly(ionic liquid) microspheres. *J. Mol. Liq.* **2022**, *362*, 119706. [CrossRef]
41. Wang, J.; Yang, D.; Feng, B.; Xiao, M.; Gai, H.; Huang, T.; Zhou, Y.; Song, H. Design of adjustable hypercrosslinked poly(ionic liquid)s for highly efficient oil-water separation. *Sep. Purif. Technol.* **2022**, *285*, 120407. [CrossRef]

42. Wei, R.; Yang, B.; He, C.; Jin, L.; Zhang, X.; Zhao, C. Versatile and robust poly(ionic liquid) coatings with intelligent superhydrophilicity/superhydrophobicity switch in high-efficient oil-water separation. *Sep. Purif. Technol.* **2022**, *282*, 120100. [CrossRef]
43. Atta, A.M.; Al-Lohedan, H.A.; Ezzat, A.O. Synthesis and application of geminal dicationic ionic liquids and poly(ionic liquids) combined imidazolium and pyridinium cations as demulsifiers for petroleum crude oil saline water emulsions. *J. Mol. Liq.* **2021**, *325*, 115264. [CrossRef]
44. Deng, X.; Zhang, J.; Zhang, L.; Cheng, G.; Chen, B.; Zhang, Y.; Gao, G. Poly(ionic liquid)-Coated Meshes with Opposite Wettability for Continuous Oil/Water Separation. *Ind. Eng. Chem. Res.* **2020**, *59*, 6672–6680. [CrossRef]
45. Zhang, X.; Chen, Q.; Wei, R.; Jin, L.; He, C.; Zhao, W.; Zhao, C. Design of poly ionic liquids modified cotton fabric with ion species-triggered bidirectional oil-water separation performance. *J. Hazard. Mater.* **2020**, *400*, 123163. [CrossRef]
46. Zhang, X.; Mo, Z.; Arenal, R.; Li, W.; Wang, C. Efficient oil-water separation by a robust superhydrophobic coating prepared directly from commercial lacquer using silanized multi-walled carbon nanotubes as filler. *Appl. Surf. Sci.* **2023**, *609*, 155208. [CrossRef]
47. Du, X.; You, S.; Wang, X.; Wang, Q.; Lu, J. Switchable and simultaneous oil/water separation induced by prewetting with a superamphiphilic self-cleaning mesh. *Chem. Eng. J.* **2017**, *313*, 398–403. [CrossRef]
48. Sun, Y.; Liu, Y.; Xu, B.; Chen, J.; Yuan, W.; Jiang, C.; Wang, D.; Wang, H. Simultaneously achieving high-effective oil-water separation and filter media regeneration by facile and highly hydrophobic sand coating. *Sci. Total Environ.* **2021**, *800*, 149488. [CrossRef]
49. Udomsin, J.; Hu, C.; Wang, C.; Chen, J.; Tsai, H.; Kuo, S.; Hung, W.; Lai, J. Constructing Superwetting Membranes by Sodium Lignosulfonate-Modified Carbon Nanotube for Highly Efficient Crude Oil-In-Water Emulsions Separations. *Sep. Purif. Technol.* 2023; *in press*. [CrossRef]
50. Zhang, Y.; Gong, X. Smart and durable pH-responsive superhydrophobic fabrics with switchable surface wettability for high-efficiency and complex oil/water separation. *Giant* **2023**, *14*, 100157. [CrossRef]
51. Li, S.; Zhang, L.; Qin, Z.; Zhou, L.; Lv, T.; Wu, F.; Liu, Z.; Zhao, C.; Yu, C.; Xing, G. Hydrophobic Ti_3C_2Tx/PU sponge prepared from commercial amphiphilic PU sponge for oil/water separation with ultrahigh flux. *J. Environ. Chem. Eng.* **2022**, *10*, 108542. [CrossRef]
52. Itoh, Y.; Chen, S.; Hirahara, R.; Konda, T.; Aoki, T.; Ueda, T.; Shimada, I.; Cannon, J.J.; Shao, C.; Shiomi, J.; et al. Ultrafast water permeation through nanochannels with a densely fluorous interior surface. *Science* **2022**, *376*, 738–743. [CrossRef] [PubMed]